UNIVERSITY OF CALIFORNIA,
IRVINE

The Effect of Discontinuous Electrical Propagation on Contractile Stress in Cardiac Muscle

THESIS

submitted in partial satisfaction of the requirements
for the degree of

MASTER OF SCIENCE
in Biomedical Engineering

by

Evan Jonathan Bender

Thesis Committee:
Professor Anna Grosberg, Chair
Professor Wendy Liu
Professor Timothy Downing

2020

DEDICATION

To

my family

in recognition of hard work, determination, and sacrifice

they cared for me in every way possible and shaped me into the person I am today

TABLE OF CONTENTS

LIST OF FIGURES

LIST OF TABLES

ACKNOWLEDGEMENTS

I would like to express my sincerest appreciation to my committee chair, Professor Anna Grosberg, who has continually offered her support and guidance throughout my graduate school journey. It was by her example that I strived for excellence whilst conducting research into this subject matter.

I would also like to thank my committee members, Professor Wendy Liu and Professor Timothy Downing, for offering their feedback and assistance with the thesis submission process.

I would like to thank the entire Cardiovascular Modeling Lab for their support, guidance, and fond memories during our time together. In particular, I thank Jasmine Naik for time spent training me and insight into experimental backgrounds. I thank Mehrsa Mehrabi for the knowledge and opportunity to work in stem cell culture. I thank William Sherman for assisting me in micropattern design. Lastly, I thank Emil Lundqvist, Huiyi (Cathy) Yang, Mohamed Ajam and Richard Tran for helping me with daily tasks, allowing me to complete this work in a timely manner.

ABSTRACT OF THE THESIS

The Effect of Discontinuous Electrical Propagation on Contractile Stress in Cardiac Muscle

By

Evan Jonathan Bender

Master of Science in Biomedical Engineering

University of California, Irvine, 2020

Professor Anna Grosberg, Chair

Through the creation of *in vitro* and *in silico* models of discontinuous electrical propagation, data can be collected about the stress generation of sarcomeres in abnormal cardiac tissues. Diseased and malformed cardiac muscle causes improper spread of action potentials, thus inhibiting normal cardiac contractile function. Biomedical solutions to common cardiovascular problems would benefit from a reproducible model. Here, we create a model to collect contractile force data in discontinuous engineered cardiac tissues *in vitro* and confirm theoretical predictions about the effect of discontinuity on stress generation. The formulation of a computational model about the probability of sarcomere firing events is also discussed, together with the methods of how this model will be validated by the *in vitro* model. While further development and experimental testing is needed, these designs are an efficient way to measure structure-function relationships in irregular cardiac muscle.

Chapter 1: Introduction

Cardiac impulse propagation plays a major role in the structure and function of the human heart. Proper physiological propagation occurs between cardiac cells that are electrically coupled via functional gap junctions [1-3]. Diseased tissue can create discontinuities in the electrical pathways that are formed by gap junctions. Also, gap junctions may not form properly during cell differentiation in neonates, causing myocardial synchronization to be hindered [4,5]. The most abundant gap junction protein, connexin43 (Cx43), is down regulated in regions of ventricular remodeling due to scar tissue formation or fibrosis [3,6]. Loss of Cx43 expression, increased tissue stiffness, and many other factors may result in conduction abnormalities and contractile dysfunction that can contribute to arrhythmogenesis [3,6,7]. To better understand the effect of improper impulse propagation on stress generation, a model of electrical discontinuity in cardiac tissue is needed. This model will help predict both the value and profile of contractile force generated by cardiac muscle. Biomedical solutions to common cardiovascular diseases due to loss of electrical and mechanical functionality will significantly benefit from a reproducible experimental model.

In vivo models of electrical discontinuity are not feasible because reproducing the same experimental conditions in the heart for multiple test trials on animal subjects is impossible. *In vitro* models using engineered tissue designs have the potential for higher throughput and higher quality data needed for successful early-stage testing [8]. Previous studies of communication between cardiomyocytes focus mostly on mechanical deformations or electrical propagation through differing cell types [9-12]. These models give insight into synchronization of isolated or neighboring cells, but do not offer much detail about the contractile force profiles of discontinuous engineered cardiac tissues. Alternatively, using microcontact printing techniques, anisotropically

aligned cardiomyocyte monolayers can be constructed with built-in gaps, which closely mimics native cardiac cell orientation and provides electrical discontinuity without other cell types between tissue segments [13]. We expect that the cooperative forces generated under these conditions will be significantly decreased from those of continuous tissues. To verify this prediction, a platform for measuring the magnitude and trace of contractile force is necessary.

The muscular thin film (MTF) technology developed by Feinberg et al and Grosberg et al allows for a highly customizable, high throughput approach to testing electrical propagation and contractility in cardiac tissue [8,13]. By combining our micropatterning design with MTFs, we can measure the stress of bending films to learn about the synchronization of separate regions of tissue. We can then test our model to confirm the theoretical prediction that as the number of electrically independent segments (N) of tissue increases, the maximum contractile stress (σ) decreases in proportion to $1/\sqrt{N}$.

Building upon the framework from past studies, we identified a need for a theoretical model of cardiac firing events, which would offer preliminary results about the effect of propagation on stress generation. As an alternative to other simulations that focus on chemical reactions or mechanical properties, we are developing an *in silico* model that provides predictions about the probability density of sarcomere firing events and their related stress profiles [14,15]. We aim to validate this model by comparing the predicted stress profiles to those obtained from our experimental testing on MTFs. In the following chapters, we discuss the methods and design of our model, as well as the experimental procedures that allow us to validate our theoretical prediction. We also discuss future directions in which we hope to expand our predictions to other cell types in order to comment on electrophysiological mechanisms.

Chapter 2: Contractility Model

Described in this chapter are the methods particular to the experimental contractility model. MTF experiments are still ongoing. The following results are the design process, preliminary data achieved so far, and the future work to further test our design.

Methods

Substrate fabrication

Muscular thin films (MTFs) were made via a multi-step process on rectangular glass cover slips (ThermoFisher Scientific, Hanover Park, IL), as previously described in Drew et al [16]. Large glass sections were sonicated in 95% ethanol for 30 min and incubated in a 65°C oven for at least 30 min. The glass sections were then covered in protective film, which was cut and removed using custom templates to provide strips of exposed glass. Each strip varied in size according to the desired length of the MTF, which corresponded to the number of electrically independent segments on a given film. Next, poly(N-isopropylacrylamide) (PIPAAm; Polysciences, Warrington, PA) was spin coated onto the exposed glass strips and allowed to dry at room temperature for at least 15 min. The remaining protective film was removed, and the entire glass section was spin coated with polydimethylsiloxane (PDMS; Ellsworth Adhesives, Germantown, WI) mixed at a 10:1 ratio with curing agent. The glass sections were moved to a 65°C oven overnight to cure. Lastly, the glass sections were cut into individual 12 mm × 14 mm cover slips using a diamond cutter.

Silicon wafer fabrication

Stamp patterns were designed in Adobe Illustrator software (Adobe Systems, San Jose, CA). Patterns were made to be 1.5 cm × 1.5 cm with 20 μm wide lines and 5 μm gaps between lines in segments of either 250 μm or 500 μm with 50 μm gaps between segments for aligned anisotropic tissue. Designs were etched into 5 in × 5 in chrome with soda-lime glass photomasks by a third-party vendor (FrontRange Photomask, Lake Havasu City, AZ). Silicon wafers were made through SU-8 deposition using the glass masks in the Bio-Organic Nanofabrication Facility (University of California, Irvine, Irvine, CA).

Micropatterning extracellular matrix

Stamps were prepared as previously described in Knight et al [17]. Silicon wafers were covered in 60-80 g of PDMS. They were degassed then cured overnight in a 65°C oven. Thereafter, the PDMS was peeled off the wafers, and the square patterned regions were cut out and stored for use.

Stamps were sonicated in 95% ethanol for 15 min and were dried in a biosafety cabinet under sterile conditions using compressed nitrogen. Next, stamps were coated with a 0.1 mg/mL concentration of fibronectin (FN; ThermoFisher Scientific, Hanover Park, IL) and allowed to incubate at room temperature for 1 h. After 1 h incubation, stamps were dried using compressed nitrogen and stamped onto PDMS coated coverslips that had been exposed to UV light (Jelight Company, Irvine, CA) for 8 min. The stamped coverslips were submerged in solution (5 g Pluronics F-127, dissolved in 500 mL sterile water; Sigma-Aldrich, St. Louis, MO) for 5 min and were immediately rinsed three times with room temperature phosphate-buffered saline (PBS;

ThermoFisher, Grand Island, NY). Following the last wash, coverslips were left submerged in PBS, and the plate was wrapped in parafilm for storage until seeding.

Myocyte harvest, seeding, and culture

As described in Knight et al [17], neonatal rat ventricular myocytes (NRVMs) were isolated from 2-day-old neonatal rats (Charles River Laboratories, Wilmington, MA). Briefly, ventricular myocardium was excised under sterile conditions in a biosafety cabinet, rinsed in Hanks balanced salt solution buffer (HBSS; ThermoFisher, Grand Island, NY), and then incubated in a 1 mg/mL trypsin solution (Sigma-Aldrich, St. Louis, MO) dissolved in HBSS at 4°C overnight (12 h). The trypsin solution was then removed and tissue was neutralized in warmed M199 culture medium (Invitrogen, Carlsbad, CA) supplemented with 10% heat inactivated Fetal Bovine Serum (FBS), 10 mM HEPES, 20 mM glucose, 2 mM L-glutamine (ThermoFisher, Grand Island, NY), 1.5 mM vitamin B-12 and 50 U/mL penicillin (Sigma-Aldrich). Media was removed without disturbing tissue, which was dissociated through several washes of 1 mg/mL collagenase dissolved in HBSS. Next, collagenase cell solutions were centrifuged at 1200 rpm for 10 min. The supernatant was then aspirated, and cells were resuspended in chilled HBSS. The HBSS cell solution was then centrifuged again at 1200 rpm for 10 min. The supernatant was aspirated, and cells were resuspended in warm 10% M199 media. The cell solution was purified through three consecutive pre-plates of 45, 45, and 40 min in cell culture flasks (BD Biosciences, San Diego, CA) in an incubator. After the final pre-plate, cells were counted using a disposable hemocytometer (ThermoFisher Scientific, Waltham, MA) and were seeded at a density of 4.0×10^5 cells per 3 mL. At 24 h after seeding, dead cells were rinsed from substrates with warmed PBS

three times. After washing, warm 10% M199 was added, and substrates were returned to the incubator. Then 24 h later, 10% M199 was replaced with warm 2% M199 media.

Contractility experiments

MTF experiments were performed 4 days after seeding in warmed (37°C) Normal Tyrode's solution of 5 mM HEPES, 1 mM magnesium chloride and 5 mM glucose, 1.8 mM calcium chloride, 5.4 mM potassium chloride, 135 mM sodium chloride, and 0.33 mM sodium phosphate (Sigma Aldrich, St. Louis, MO). First, patterned substrates were placed into Petri dishes with warmed Normal Tyrode's solution. Then, substrates were cut into thin films using a razor blade. Two cuts were made perpendicular to tissue direction at the edge of the PIPPAm-coated region, approximately 1 mm apart. The resulting strip was then peeled away using tweezers. 6 to 8 more cuts were made parallel to tissue direction, first spaced about 1 mm apart, then spaced about 3 mm from that and so on. A scalpel was used to cut at the base of the thinner strips, which were then peeled away with tweezers. These cuts resulted in 3 to 5 films about 3 mm in width fixed on one edge to the substrate. The length of the film depended on the width of the PIPPAm layer that was coated onto substrates, with the films always spanning the entire PIPPAm layer.

The Tyrode's solution in the dish cooled to room temperature, allowing the MTFs to gently peel up as the PIPPAm dissolved. MTFs were then transferred to 35 mm Petri dishes with fresh Normal Tyrode's solution inside of a temperature-controlled incubator. Customized electrodes were affixed to the dish, sitting across the base of the row of films. Negative control substrates were paced at a range of 0.5-2.5 Hz in increments of 0.5 Hz at 10 V using an external field stimulator (Myopacer, IonOptix Corp., Milton, MA). Experimental group films were not paced and left to spontaneously beat at will. Short video clips (6 s duration) for each sample were

captured using a model number SZX9 Stereoscope (Olympus America, Center Valley, PA) mounted with a model number acA1300-200um camera (Basler, Exton, PA).

Fixing and immunostaining

Fixing occurred 4 days after seeding. Wells were fixed in warmed (37°C) 4% paraformaldehyde (PFA; VWR, Radnow, PA) combined with 0.001% Triton X-100 (Sigma Aldrich, St. Louis, MO) for 10 min. Next, wells were washed three times in room temperature PBS for 5 min each wash.

Next, cells were immunostained by incubating seeded cover slips for 1 h at room temperature in primary antibodies for actin (Alex Fluor 488, Phalloidin; ThermoFisher, Grand Island, NY), sarcomeric α-actinin (Mouse Monoclonal Anti-α-actinin; Sigma-Aldrich), nuclei (4',6'-diaminodino-2-phenylinodole, DAPI; ThermoFisher, Grand Island, NY), and FN (polyclonal rabbit anti-human fibronectin; Sigma-Aldrich, St. Louis, MO). After incubation, samples were washed three times in PBS to prevent background staining. Samples were then secondary stained by incubating for 1 h at room temperature in tetramethylrhodamine-conjugated goat anti-mouse IgG antibody (Alexa Fluor 633 Goat Anti-Mouse, ThermoFisher, Grand Island, NY) and tetramethylrhodamine-conjugated goat anti-rabbit IgG antibody (Alexa-Fluor 750 Goat Anti-Rabbit, ThermoFisher, Grand Island, NY). Once again, samples were washed three times in PBS and mounted on glass microscope slides with Prolong Gold Antifade reagent (ThermoFisher, Grand Island, NY). Clear nail polish was applied around the edges of coverslips to seal them onto microscope slides, then slides were left overnight to dry under an opaque container to protect from light. After, microscope slides were stored at -20°C until imaging.

Imaging and imaging analysis

Immunostained cells were imaged with an IX-83 inverted motorized microscope (Olympus America, Center Valley, PA). Images were taken using an UPLFLN 40x oil immersion objective (Olympus America, Center Valley, PA) and a digital CCD camera ORCA-R2 C10600-10B (Hamamatsu Photonics, Shizuoka Prefecture, Japan). Ten fields of views were selected at random for each sample and imaged at 40x magnification (6.22 μm/pixel).

MTF video clips were analyzed using custom ImageJ and Matlab software, as previously described in Knight et al [17]. Film bending was tracked for each sample, and diastole (defined by the longest projection of each film) and systole (defined by the shortest projection of each film) were automatically detected. Each video was labeled with the original length of each film as indicated by a pink outline and film tracking was indicated by an orange bar. Active stress was defined as the difference between systole and diastole for each film. Cell and substrate thicknesses are important parameters in the calculation of muscular thin film contractility. Cell thicknesses for each tissue type were measured, and the average cell thickness for each tissue type was used in thin film analysis. Substrate thickness was measured for each chip preparation using a DektakXT profilometer (Bruker, Tucson, AZ).

Results

MTF architecture

Muscular thin films are useful for measuring the contractile force of segments of engineered cardiac tissues *in vitro*. We can use this force data to help characterize the mechanical cooperation of myocytes that are electrically coupled. In order to test the effect of discontinuity on stress in cardiac tissue, we created gaps in the NRVM monolayer on each thin film. Previous work

by the Parker group established that the contractile stress of a sarcomere, $\sigma_{sarcomere}$, increases with uniaxial sarcomere alignment, and that resultant tissue contractility is directly dependent on the cellular and subcellular architecture [18]. While we kept this anisotropic alignment in our micropattern designs, we sought to determine the MTF length necessary to accommodate a maximum of 16 electrically independent tissue segments. This is based on our theoretical prediction that the maximum contractile stress (σ) of each film is proportional to the number of electrically independent segments (N):

$$\sigma = \frac{1}{\sqrt{N}}\sigma_0. \quad (1)$$

Therefore, we expected the maximum contractile stress of our films to follow the function:

$$\sigma = \frac{1}{\sqrt{16}}\sigma_0 = \frac{1}{4}\sigma_0 \quad (2)$$

In addition, we aimed to create a PDMS substrate thickness that would result in similar film stress values (~15-25 kPa) as previously reported [19]. A range of experimental values for film length, thickness, and stress were visualized in Matlab (Fig. 1). This data was modeled to be consistent with MTF constructs with a continuous cardiomyocyte layer. Therefore, ranges of

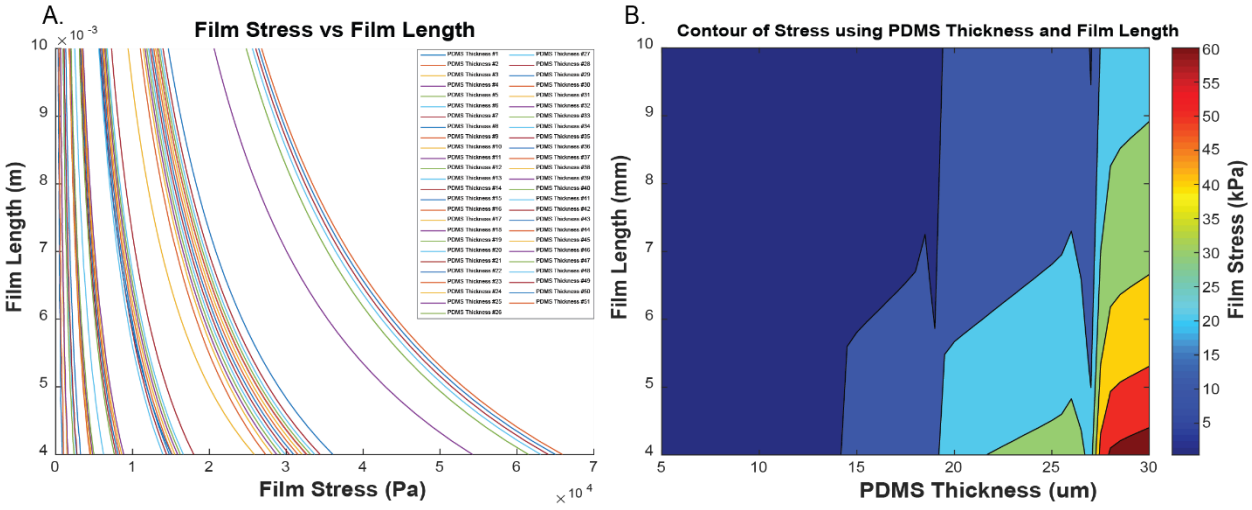

Figure 1: Calculated MTF Parameters. (A) Plot of possible film lengths vs calculated stress values (Eq. 1) for every PDMS thickness. (B) Contour plot of calculated stress values for corresponding possible film lengths and PDMS substrate thicknesses.

thicknesses and lengths were picked knowing that stress values for our discontinuous MTFs should be lower for comparable values.

We considered the upper and lower limits of films lengths that were feasible for producing data. Any films that were long enough so that the radius of curvature reached 2π were not analyzable [8]. Similarly, we reasoned that very short films (<1 mm) would not produce a sufficient deformation for analysis. Based on these assumptions, a range of lengths was created (Table 1) for both short and long versions of MTFs by multiplying the total length of the tissue segment plus the gap by the number of desired segments. Long versions used tissue segments of 500 µm with 50 µm gaps, giving a range of 2.2 mm to 8.8 mm for desired testing lengths. Short versions used tissue segments of 250 µm with 50 µm gaps, giving a range of 1.2 mm to 4.8 mm for desired testing lengths. Film thicknesses were chosen in the range of 15 µm to 30 µm. These values were theoretical aims, and experimental thickness values were measured during testing.

Table 1: Film Segment Lengths. List of chosen MTF segment variations and corresponding lengths.

250 µm pattern		500 µm pattern	
# segments	Length (mm)	# segments	Length (mm)
4	1.200	4	2.200
6	1.800	6	3.300
9	2.700	9	4.950
12	3.600	12	6.600
16	4.800	16	8.800

A photomask with our design specifications was created and used to make silicon wafers featuring these patterns (Fig. 2A). Using the desired ranges for MTF length, long and short segment patterns were created in Adobe Illustrator software (Fig. 2B & 2C), both featuring 20 µm wide

lines and 5 µm gaps between lines for anisotropic alignment (Fig. 2D). In addition, customized transparency designs were created in Adobe Illustrator to reflect updated area sizes for spin coating PDMS and PIPPAm onto glass coverslips. Experiments are still ongoing, so optimized film lengths and thicknesses are yet to be determined for discontinuous engineered tissues.

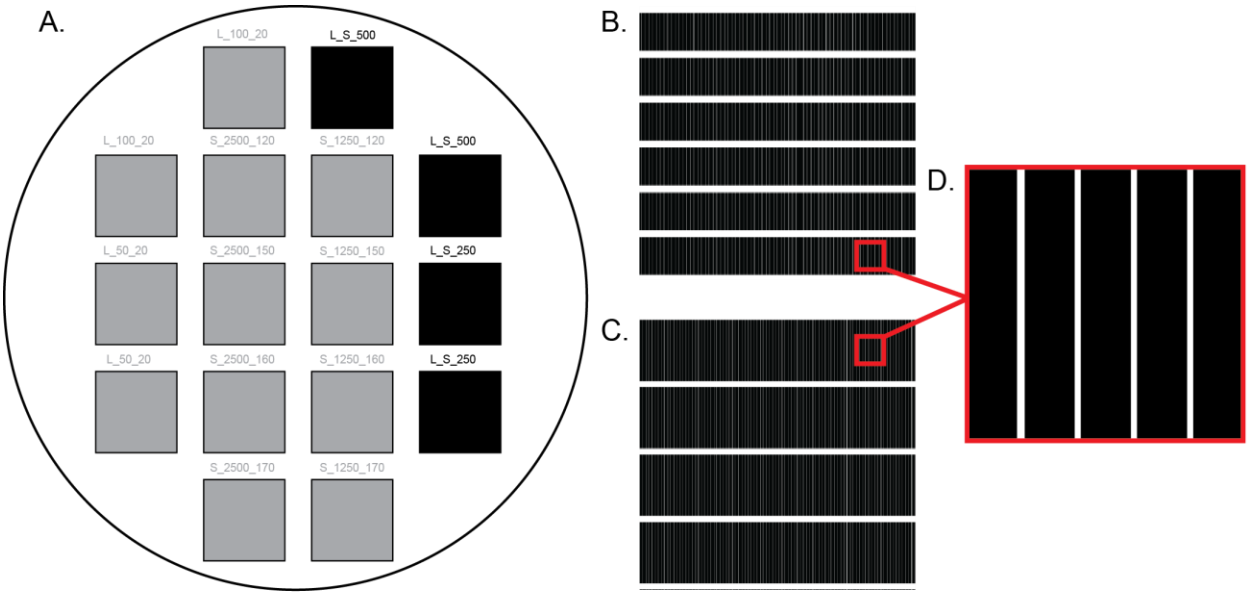

Figure 2: Silicon Wafer & Stamp Pattern. (A) Wafer schematic featuring micropatterns for discontinuous tissue segments (black), and other projects by the Grosberg group (grey). (B) Line segments 250 (L_S_250) pattern: 250 µm tissue segments x 50 µm gaps. (C) Line segments 500 (L_S_500) pattern: 500 µm tissue segments x 50 µm gaps. (D) 20 µm wide lines x 5 µm gaps for anisotropic cardiomyocyte organization via FN functionalization of PDMS-coated glass coverslips.

Validation of experimental conditions

Before MTF experiments could begin, validation of micropatterns was required. PDMS stamps were created and checked under a microscope for visual defects. It was possible that stamps did not degas properly before curing. This led to bubble formation on stamp surfaces, causing improper fibronectin functionalization of coverslips during microcontact printing. Any stamps exhibiting these features were remade. Once acceptable stamps were made, PDMS-coated glass coverslips were stamped and seeded at 4.0×10^5 cells per 3 mL for 2D validation cultures. Initial fluorescence imaging showed that fibronectin lines were properly imprinting onto coverslips (Fig.

3A), but cardiomyocytes were not forming discrete muscle fibers as previously demonstrated (Fig. 3C & 3D) [13,18]. Instead, images showed immature sarcomeric z-line structures in individual cells, clustered together but not joined.

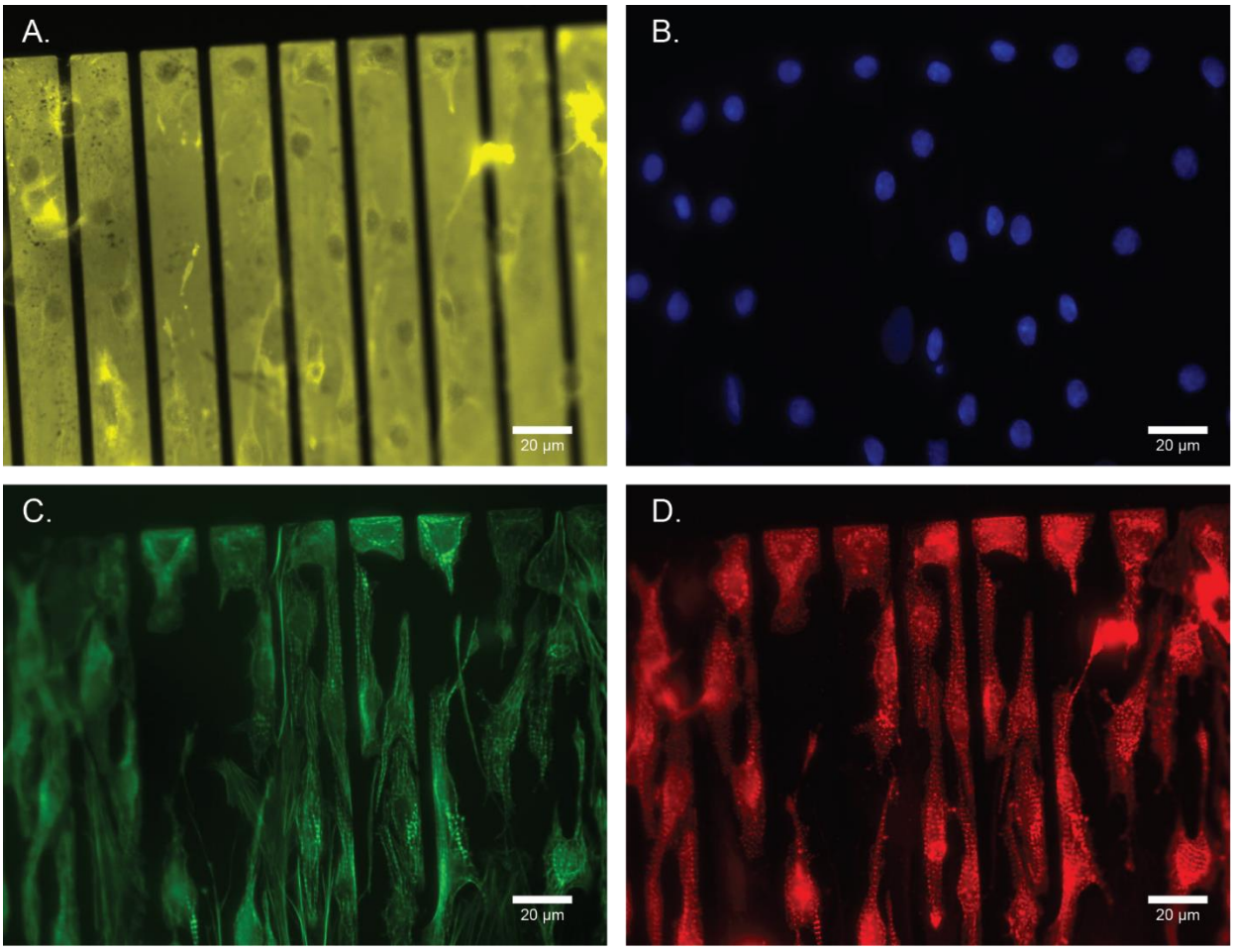

Figure 3: Micropattern Validation. (A) 20 µm x 5 µm anisotropic FN pattern showing top boundary of segment. Patterned NRVMs immunostained for (B) nuclei (blue), (C) actin (green), and (D) α-actinin (red).

We assessed that cardiomyocytes may have been over-seeded, leaving inadequate room for growth along micropatterned lines. To attempt to fix this issue, cell seeding density trials were conducted at 3.75×10^5 (375k), 4.0×10^5 (400k), and 4.25×10^5 (425k) cells per 3 mL. Images of culture wells were taken on days 1-3 after seeding. On day 1, cells in the 400k wells showed more adherence to patterned substrates, as well as morphology that more closely mimicked what we

would expect of mature cardiomyocytes (Fig. 4B) [20]. 375k and 425k wells showed decreased adherence and growth compared to 400k wells (Fig. 4A & 4C). On day 2, 400k cells had proliferated to approximately 70% confluency but still showed signs of fragmented muscle formation (Fig. 4E). 375k and 425k wells showed no growth, and there was indication that cells were starting to delaminate (Fig. 4D & 4F). By day 3, wells for all seeding densities showed cell death and unhealthy morphology (Fig. 4H-4J). We concluded that seeding density was not preventing discrete muscle fiber formation, and that 400k remained to be the best seeding density for our micropattern designs.

After ruling out seeding density, cardiomyocyte harvest troubleshooting proceeded. It was determined that stored FBS aliquots used in culture media had spoiled, resulting in improper resuspension and proliferation after seeding. A new batch of FBS was aliquoted, and a new round of cardiomyocytes was cultured for validation. Here, observations of culture wells showed beating cardiomyocytes on day 3 after seeding. Unfortunately, the samples were contaminated before data collection began, and further validation was not completed due to time constraints.

Discussion and Future Work

While data for contractility studies has not yet been collected, validation tests showed promising results. 2D culture images confirmed that spontaneous beating of cardiomyocytes on discontinuous micropatterns is possible. Therefore, further validation tests can be brief before MTF experiments can be performed. As mentioned, we do not yet fully understand the optimal length and thickness combination for MTF contraction. Alford et al previously demonstrated that higher curvatures require higher stresses for thicker substrates [19]. Combined with our discontinuous patterns, MTFs may struggle to deform spontaneously. Because spin coating PDMS

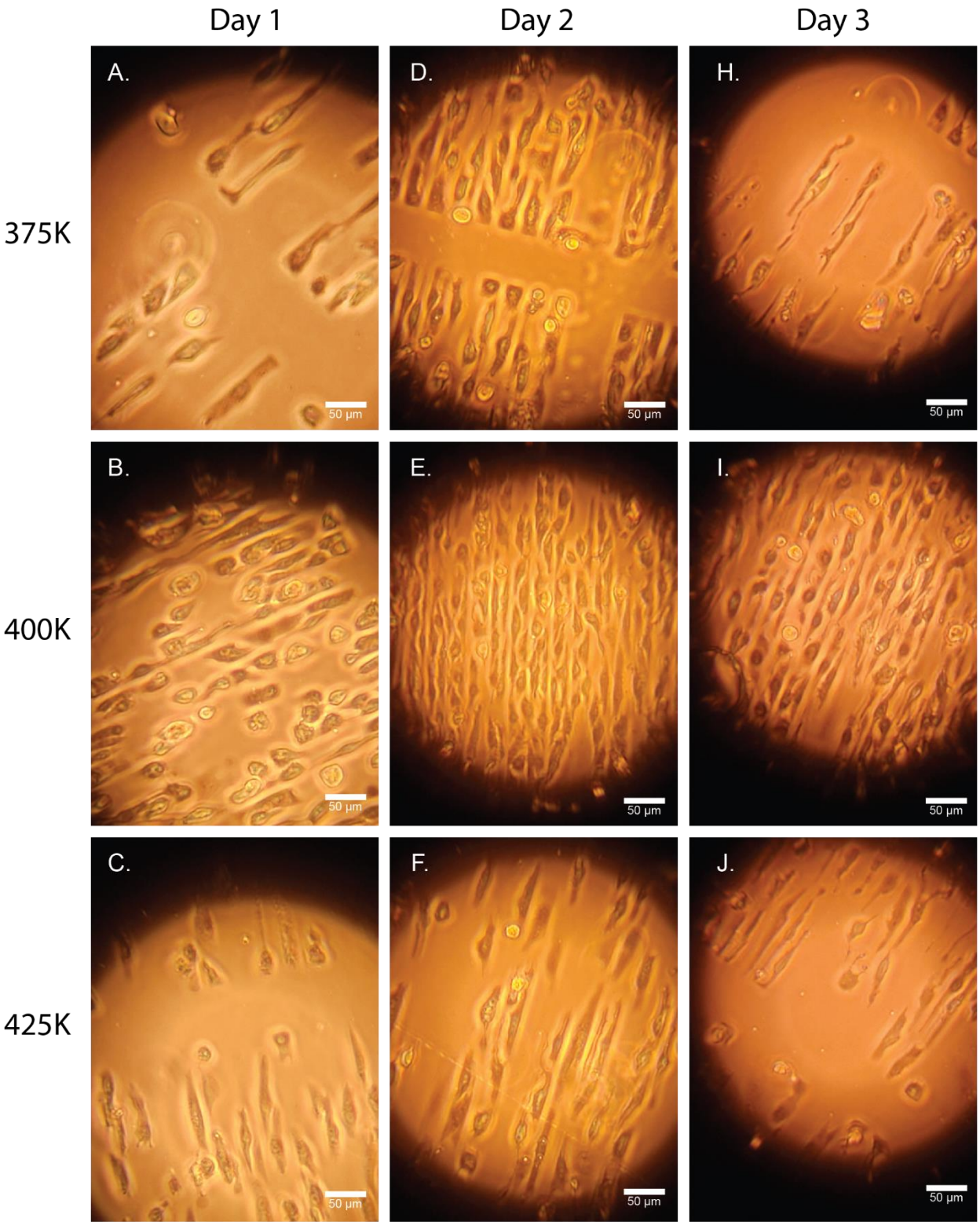

Figure 4: Seeding Density Trial. 4x images of cell densities for days 1-3 after seeding. Day 1: (A) 375k, (B) 400k, and (C) 425k. Day 2: (D) 375k, (E) 400k, and (F) 425k. Day 3: (H) 375k, (I) 400k, and (J) 425k.

is rather imprecise and thickness must be measured from sample coverslips, fine-tuning film lengths may be more feasible for controlling stresses. Reassessing the selected number of tissue segments may be an option and would help to accurately represent propagation in diseased or abnormal tissues.

With further optimization, our experimental model allows for both a structural and functional approach to understanding the effect of improper electrical propagation on contractile stress. The established MTF assay provides a high-throughput alternative to other discontinuous propagation methods [9-12,21-22]. Ultimately, this model can potentiate early-stage solutions to relevant cardiovascular diseases.

Chapter 3: Computational Model

Described in this chapter are the methods particular to the computational sarcomere firing event model. The development of this model is still ongoing. The following results are the relevant equations, preliminary data achieved so far, and the future work to further test our design.

Model Formulation

Due to unforeseen circumstances, we were forced to find an alternative method of studying the effect of electrical propagation on cardiac contractile stress. Our focus turned to computational modeling of sarcomere firing events. Previous work by Knight et al developed probability distributions as a function of sarcomere orientation [17]. Conversely, our aim is to develop probability distributions as a function of time. Data can be gathered by simulating cardiac action potentials and recording the time intervals between events. Here, our goal was to answer the question: at any given time, what is the probability of firing of any given sarcomere?

We introduced the concept of the local time of the sarcomere; that is, the elapsed time before the next probability-based firing event. To model this variable for an individual sarcomere, we considered some basic simplifications. First, before time t = 0, we assume no events take place. Second, the local time scale is reset to t = 0 whenever a firing event occurs for that sarcomere. Lastly, if the sarcomere just fired, it cannot fire again for some period of time, also known as the absolute refractory period for action potentials [1]. Together, these assumptions allow us to write the probability of sarcomere firing in the form:

$$\bar{P}(t) = \begin{cases} 0 & 0 < t \leq t_0 \\ P_2 + P_1 t & t_0 < t \leq t_1 \\ P_0 & t_1 < t \end{cases}. \qquad (3)$$

During the absolute refractory period $0 < t \leq t_0$, there is no chance of a firing event. After the end of the absolute refractory period, we say the probability increases linearly during the relative refractory period $t_0 < t \leq t_1$. During this period, action potentials can occur, but they require a larger stimulus to begin [1]. After the relative refractory period, the probability of firing levels off at a constant value, which we can say is the initial firing probability for any given sarcomere.

Creating a cycle around an individual sarcomere allows us to expand our theory to a customizable scale. If we run these simulations an infinite number of times, we can compute averages of the probability of firing and the time until the next firing event for given sarcomeres. Also, each sarcomere firing event creates a force profile with a unique magnitude and trace, and the average force is driven by how many sarcomeres are firing at any given time. If we include the micropattern specifications from our experimental MTF model, we can say that our sarcomeres are locally organized. This allows us to calculate the amount of force produced using force vector addition [17].

Results, Discussion, and Future Work

The computational model is still in early development. So far, we have enabled the use of a random number generator to simulate firing events. Binary matrices of firing states were created, allowing us to process large quantities of action potentials quickly. Further testing is still needed to validate this approach. Several aspects of the model still need to be implemented, including a spatial coordinate system and possible scenarios for the interaction between sarcomeres. Previous studies have mapped the geometry of myofibril growth [23]. Along the same lines, including vectors for position in our model would allow us to research propagation of action potentials from one sarcomere to another. Therefore, more mathematical formulation is needed to account for

probability increases due to neighboring firing events. The magnitude of these increases depends on the distance between sarcomeres.

With optimized probability functions and a spatially organized grid, this stochastic model would benefit from a map of sarcomere firing. 2D movies of color-coordinated firing states would help users visualize membrane potentials in real-time, while still providing high throughput data about impulse propagation. The Parker group has previously demonstrated the ability to simulate various MTF experiments *in silico* [24]. By implementing the micropattern designs from our experimental model into the positioning vectors, theoretical MTF contractility studies for discontinuous cardiac tissues are possible. Collecting data from simulations with discontinuity would allow us to build probability distributions of the frequency of sarcomere firing events, as well as overall contractile stress profiles for customizable sarcomere grids. Ultimately, these outputs can be compared to our *in vitro* experimental values, thus validating the *in silico* model. Together, both models offer a thorough investigation of the effect of electrical impulse propagation on generated stress in cardiomyocytes.

Chapter 4: Future Directions

Described in this chapter are the future directions of our model after validation. We introduce new experimental interests, followed by descriptions of participation on an additional project which form the foundation for these interests.

Introduction

Developing treatments for cardiovascular illnesses takes a long time due to the experimental process of designing and validating new methods. This development time can be reduced by using high-throughput models of disease. After validation, we hope to expand our contractility model to include other types of cells, such as iPSC-derived cardiomyocytes. Current studies of the Grosberg group aim to investigate the downstream mechanisms of Lamin A/C (LMNA) gene mutations in the heart [25]. These studies also apply the MTF assay to test tissue function, but they use continuous layers of iPSC-derived cardiomyocytes. Future treatments would benefit from combining aspects from the two studies. Our current contractility model will show both the magnitude and shape of force profiles that describe contractions generated by discontinuous NRVMs. Furthermore, we can test our discontinuous design with stem cell-derived tissues to attempt to match their force profiles with those of the NRVM tests. Thus, we seek to comment on the electrophysiology mechanisms of cardiac tissues of different origins. In doing so, we bring our model closer to the physiology of the human heart and further develop pathways for biomedical solutions to cardiovascular disease. In the following sections, we discuss work done on the LMNA gene mutation project that helped provide understanding for the future of the discontinuous propagation project.

Methods

Preparing well plates

10 µL/well frozen Geltrex (ThermoFisher, Grand Island, NY) was allowed to defrost on ice for 1 h. After, Geltrex was pipetted into the desired ratio of ice-cold Dulbecco's Modified Eagle's Medium (DMEM, ThermoFisher, Grand Island, NY) and gently agitated by pipetting the mixture up and down. 2 mL/well of Geltrex mixture was pipetted into 6-well plates, or 1 mL/well for 12-well plates. Plates were gently agitated to spread mixture in well and placed in an incubator for 1 h.

iPSC seeding and culture

Two iPSC lines were obtained from the Zaragoza group (UC Irvine, Irvine, CA). One cell line, patient A3, was from a family with three individuals with the heterozygous LMNA splice-site mutation. The other line, donor 2, served as unrelated negative controls without mutation. For nomenclature, patient (P) and donor (D) are followed by the family designator (A, B, or C) and the preassigned number of the individual (1, 2, 3, or 4). 490 mL Essential 8 (E8) basal media and 10 mL E8 supplement were filtered together in a filter flask. iPSCs were taken out of cryostorage and thawed in a 37°C water bath for 1-2 min. Cells were mixed gently with 10 mL complete E8 media at room temperature and centrifuged at 200xg for 2-4 min. After, supernatant was aspirated, and 2 mL/well of E8 media and 20 µL/well Revitacell (ThermoFisher, Grand Island, NY) was added to cell pellet. Cell mixture was seeded onto Geltrex plates, spread evenly over wells, and incubated at 37°C.

Cell media was changed every day with pre-warmed complete E8 media until cells reached ~80% confluency, at which point they were passaged. Media was aspirated from confluent wells

and wells were washed with Dulbecco's phosphate-buffered saline (DPBS, ThermoFisher, Grand Island, NY). 1 mL ReLeSR (StemCell Technologies, Vancouver BC, CA) was added to wells and incubated for 1 min at room temperature. Then, ReLeSR was aspirated and wells were incubated for 7 min at room temperature. After, 1 mL/well E8 media was added to wells, and plates were gently tapped to release iPSC colonies. Colonies were transferred to a 50 mL conical tube and E8 media was added based on the desired split ratio. Cell mixture was transferred to new Geltrex plates and incubated at 37°C.

iPSC singularization

At the end of passage 15, iPSC cultures were singularized for 4 days before differentiation. Media was aspirated from confluent wells and wells were washed with Dulbecco's phosphate-buffered saline (DPBS, ThermoFisher, Grand Island, NY). 1 mL/well TrypLE (ThermoFisher, Grand Island, NY) was added to 6 well plates and incubated for 5-7 min at 37°C. Plates were gently agitated to detach cell colonies and 2 mL/well E8 media was added to wells. Colonies were transferred to a 50 mL conical and centrifuged at 200xg for 4 min. After, supernatant was aspirated and cells were resuspended in E8 and counted with a hemocytometer. Seeding densities were calculated and 20 µL Revitacell (ThermoFisher, Grand Island, NY) per 2 mL cell mixture was added to cells and media. 1 mL cell suspension was seeded into Geltrex-coated 12-well plates, gently spread over wells, and incubated at 37°C. Cell media was changed every day with pre-warmed complete E8 media until differentiation.

Results and Discussion

For a period of time before starting work on the discontinuous propagation project, assistance was given on the LMNA gene mutation project in the form of iPSC culture. Cell lines were cultured up to singularization, at which point control of said cultures was given back to Ph.D. students in the Grosberg group. This process was repeated numerous times in preparation for MTF contractility studies and RNA sequencing data collection. Stem cell culture assistance was no longer provided once the propagation project had begun. The work done with these cell lines provided experience in stem cell culture methods and helped inform upon MTF contractility experiments. As a result, we developed the aforementioned ideas to incorporate iPSCs into future versions of the discontinuous propagation model. By using cells originally derived from human samples, we hope to make conclusions about the electrophysiological similarities between tissues of different origins as well as the effect of improper propagation on various cell types. These future iterations of our model will more closely mimic the native physiology of diseased human cardiac tissues, paving the way for quicker development of enhanced cardiovascular disease treatment.

References

[1] Feher, J. (2012). Quantitative human physiology an introduction (2nd ed.). Waltham, MA: Academic Press.

[2] Haraguchi, Y., Shimizu, T., Yamato, M., Kikuchi, A., & Okano, T. (2006). Electrical coupling of cardiomyocyte sheets occurs rapidly via functional gap junction formation. Biomaterials, 27(27), 4765–4774. https://doi:10.1016/j.biomaterials.2006.04.034

[3] Severs, N. J., Bruce, A. F., Dupont, E., & Rothery, S. (2008). Remodelling of gap junctions and connexin expression in diseased myocardium. Cardiovascular Research, 80(1), 9–19. https://doi.org/10.1093/cvr/cvn133

[4] Fromaget, C., Aoumari, A. E., & Gros, D. (1992). Distribution pattern of connexin 43, a gap junctional protein, during the differentiation of mouse heart myocytes. Differentiation, 51(1), 9–20. https://doi.org/10.1111/j.1432-0436.1992.tb00675.x

[5] Angst, B. D., Khan, L. U., Severs, N. J., Whitely, K., Rothery, S., Thompson, R. P., Magee, A. I., & Gourdie, R. G. (1997). Dissociated Spatial Patterning of Gap Junctions and Cell Adhesion Junctions During Postnatal Differentiation of Ventricular Myocardium. Circulation Research, 80(1), 88–94. https://doi.org/10.1161/01.RES.80.1.88

[6] Majumder, R., Engels, M. C., Vries, A. A. F. D., Panfilov, A. V., & Pijnappels, D. A. (2016). Islands of spatially discordant APD alternans underlie arrhythmogenesis by promoting electrotonic dyssynchrony in models of fibrotic rat ventricular myocardium. Scientific Reports, 6(1). https://doi.org/10.1038/srep24334

[7] Peters, N. S., Green, C. R., Poole-Wilson, P. A., & Severs, N. J. (1993). Reduced content of connexin43 gap junctions in ventricular myocardium from hypertrophied and ischemic human hearts. Circulation, 88(3), 864–875. https://doi.org/10.1161/01.CIR.88.3.864

[8] Grosberg, A., Alford, P. W., Mccain, M. L., & Parker, K. K. (2011). Ensembles of engineered cardiac tissues for physiological and pharmacological study: Heart on a chip. Lab on a Chip, 11(24), 4165. https://doi.org/10.1039/C1LC20557A

[9] Gaudesius, G., Miragoli, M., Thomas, S. P., & Rohr, S. (2003). Coupling of Cardiac Electrical Activity Over Extended Distances by Fibroblasts of Cardiac Origin. Circulation Research, 93(5), 421–428. https://doi.org/10.1161/01.RES.0000089258.40661.0C

[10] Tang, X., Bajaj, P., Bashir, R., & Saif, T. A. (2011). How far cardiac cells can see each other mechanically. Soft Matter, 7(13), 6151. https://doi.org/10.1039/C0SM01453B

[11] Nitsan, I., Drori, S., Lewis, Y. E., Cohen, S., & Tzlil, S. (2016). Mechanical communication in cardiac cell synchronized beating. Nature Physics, 12(5), 472–477. https://doi.org/10.1038/nphys3619

[12] Cohen, O., & Safran, S. A. (2016). Elastic interactions synchronize beating in cardiomyocytes. Soft Matter, 12(28), 6088–6095. https://doi.org/10.1039/C6SM00351F

[13] Feinberg, A. W., Feigel, A., Shevkoplyas, S. S., Sheehy, S., Whitesides, G. M., & Parker, K. K. (2007). Muscular Thin Films for Building Actuators and Powering Devices. Science, 317(5843), 1366–1370. https://doi.org/10.1126/science.1146885

[14] Awrejcewicz, J., Lind, Y. B., & Kazakova, D. S. (2012). Modeling of Sarcomere Contraction Kinetics. Differential Equations and Dynamical Systems, 21(1-2), 15–19. https://doi.org/10.1007/s12591-012-0115-9

[15] Chapin, L. M., Edgar, L. T., Blankman, E., Beckerle, M. C., & Shiu, Y. T. (2014). Mathematical Modeling of the Dynamic Mechanical Behavior of Neighboring Sarcomeres in Actin Stress Fibers. Cellular and Molecular Bioengineering, 7(1), 73–85. https://doi.org/10.1007/s12195-013-0318-3

[16] Drew, N. K., Johnsen, N. E., Core, J. Q., & Grosberg, A. (2016). Multiscale Characterization of Engineered Cardiac Tissue Architecture. Journal of Biomechanical Engineering, 138(11), 111003-111003–111008. https://doi.org/10.1115/1.4034656
[17] Knight, M. B., Drew, N. K., McCarthy, L. A., & Grosberg, A. (2016). Emergent Global Contractile Force in Cardiac Tissues. Biophysical Journal, 110(7), 1615–1624. https://doi.org/10.1016/j.bpj.2016.03.003
[18] Feinberg, A. W., Alford, P. W., Jin, H., Ripplinger, C. M., Werdich, A. A., Sheehy, S. P., Grosberg, A., & Parker, K. K. (2012). Controlling the contractile strength of engineered cardiac muscle by hierarchal tissue architecture. Biomaterials, 33(23), 5732–5741. https://doi.org/10.1016/j.biomaterials.2012.04.043
[19] Alford, P. W., Feinberg, A. W., Sheehy, S. P., & Parker, K. K. (2010). Biohybrid thin films for measuring contractility in engineered cardiovascular muscle. Biomaterials, 31(13), 3613–3621. https://doi.org/10.1016/j.biomaterials.2010.01.079
[20] Jacot, J. G., Mcculloch, A. D., & Omens, J. H. (2008). Substrate Stiffness Affects the Functional Maturation of Neonatal Rat Ventricular Myocytes. Biophysical Journal, 95(7), 3479–3487. https://doi.org/10.1529/biophysj.107.124545
[21] Spach, M.S., & Kootsey, J. M. (1983). The nature of electrical propagation in cardiac muscle. *American Journal of Physiology – Heart and Circulatory Physiology*, 244(1), H3-H22. https://doi.org/10.1152/ajpheart.1983.244.1.H3
[22] Kohl, P., Camelliti, P., Burton, F. L., & Smith, G. L. (2005). Electrical coupling of fibroblasts and myocytes: relevance for cardiac propagation. Journal of Electrocardiology, 38(4), 45–50. https://doi.org/10.1016/j.jelectrocard.2005.06.096
[23] Grosberg, A., Kuo, P.-L., Guo, C.-L., Geisse, N. A., Bray, M.-A., Adams, W. J., Sheehy, S. P., & Parker, K. K. (2011). Self-Organization of Muscle Cell Structure and Function. PLoS Computational Biology, 7(2). https://doi.org/10.1371/journal.pcbi.1001088
[24] Böl, M., Reese, S., Parker, K. K., & Kuhl, E. (2008). Computational modeling of muscular thin films for cardiac repair. Computational Mechanics, 43(4), 535–544. https://doi.org/10.1007/s00466-008-0328-5
[25] Mehrabi, M., Asad, M., Becker, D., Widyastuti, H., Nguyen, C., Mccarthy, L. A., Zaragoza, M. V., & Grosberg, A. (2018). Abstract 207: In Vitro Modeling of Variable Heart Diseases Due to Lamin A/C Mutation via Patient induced Pluripotent Stem Cell Derived Cardiomyocytes. Circulation Research, 123(Suppl_1). https://doi.org/10.1161/res.123.suppl_1.207